# Electronic Structure of Mercury*

S. C. KEETON AND T. L. LOUCKS
*Institute for Atomic Research and Department of Physics, Iowa State University, Ames, Iowa*
(Received 7 June 1966)

A theoretical study of the electronic structure of crystalline mercury has been made. The energy bands were calculated using the relativistic augmented-plane-wave method. They were found to be free-electron-like with splittings due to the crystal potential and the spin-orbit interaction. The Fermi surface is quite similar to the model proposed by Brandt and Rayne and is in agreement with de Haas–van Alphen, magnetoresistance, and cyclotron-resonance data. The filled *d* band was found to be higher in energy than might at first be expected. This is explained as an indirect relativistic effect due to the fact that a relativistically self-consistent atomic potential was used in the construction of the muffin-tin potential for the crystal. Experimental evidence which supports the location of the *d* bands relative to the conduction band can be found in the optical reflectivity measurements made on the liquid state.

## I. INTRODUCTION

UNTIL very recently there had been very little experimental work relating directly to the Fermi surface of mercury. In 1947 Pippard[1] reported anomalous-skin-effect results. The de Haas–van Alphen (dHvA) effect in mercury was first reported in 1951 by Verkin, *et al.*[2] and in 1952 by Shoenberg.[3] In 1963 Gustafson, *et al.*[4] presented results for position annihilation in liquid and solid mercury. However, the orientation of the crystals in these early experiments was not known. It was not until 1965 that Brandt and Rayne[5] reported dHvA data on oriented single crystals which provided detailed information on the Fermi surface. They proposed a model of the Fermi surface which was a slight modification of the free-electron surface. It was pointed out by these authors that this model should support a set of open orbits. The same year Dixon and Datars[6] found experimental evidence of these open orbits in their transverse-magnetoresistance data. They also reported effective masses from Azbel'-Kaner cyclotron-resonance measurements which were consistent in angular dependence with the model proposed by Brandt and Rayne. Dishman and Rayne[7] have presented additional transverse magnetoresistance results which indicate the existence of a second set of open orbits which are also consistent with the proposed model. A more complete report of the dHvA effect has recently been prepared by Brandt and Rayne.[8] They have determined the topology and size of the Fermi surface from their data using a three-parameter model based on the pseudopotential method.

In this paper we report the results of an energy-band calculation for mercury using the method of relativistic augmented plane wave (RAPW).[9] This is followed by a discussion of the various experimental results (including some information on the liquid state) and their relationship to the theoretical calculation.

## II. THEORETICAL PROCEDURE

The alpha phase of mercury has a rhombohedral crystal structure. Discussions of this structure and the corresponding Brillouin zone can be found in several text books.[10–12] The lattice is composed of three equal crystallographic axes inclined to each other at the same angle $\alpha$. The fcc lattice is a special case of this in which $\alpha=60°$. For mercury $\alpha=70°44.6'$ at 5°K with the lattice constant equal to 5.643 a.u.[13,14] The Brillouin zone is shown in Fig. 1. In the fcc Brillouin zone the faces containing the points $T$ and $L$ are both regular hexagons of the same size and distance from the center of the zone $\Gamma$; the face containing the point $X$ is square. The distortion from fcc has the effect of pushing the $L$ faces closer to $\Gamma$ and the $T$ faces further away until the distances $\Gamma T$ and $\Gamma X$ are almost exactly equal and about 25% greater than the distance $\Gamma L$. An atom in the fcc lattice has 12 nearest neighbors, whereas in the rhombohedral lattice of mercury these 12 atoms separate into two sets (six atoms each) which differ in distance from the central atom by about 15%. Worster and March[15] have investigated the stability of solid mercury using pair potentials derived from structure data for the liquid and found the fcc and rhombohedral lattices

* Work was performed in the Ames Laboratory of the U. S. Atomic Energy Commission. Contribution No. 1889.
[1] A. B. Pippard, Proc. Roy. Soc. (London) **A191**, 385 (1947).
[2] B. I. Verkin, B. G. Lazarev, and N. S. Rudenko, Dokl. Akad. Nauk, SSSR **80**, 45 (1951).
[3] D. Shoenberg, Phil. Trans. **A245**, 1 (1952).
[4] D. R. Gustafson, A. R. Mackintosh, and D. J. Zaffarano, Phys. Rev. **130**, 1455 (1963).
[5] G. B. Brandt and J. A. Rayne, Phys. Letters **15**, 18 (1965).
[6] A. E. Dixon and W. R. Datars, Solid State Commun. **3**, 377 (1965).
[7] J. M. Dishman and J. A. Rayne, Phys. Letters **20**, 348 (1966).
[8] G. B. Brandt and J. A. Rayne, Phys. Rev. **148**, 644 (1966).
[9] T. L. Loucks Phys. Rev. **139**, A1333 (1965).
[10] N. F. Mott and H. Jones, *The Theory of Metals and Alloys* (Dover Publications, Inc., New York, 1958), p. 165.
[11] H. Jones, *The Theory of Brillouin Zones and Electronic States in Crystals* (North-Holland Publishing Company, Amsterdam, 1960), p. 58.
[12] J. C. Slater, *Quantum Theory of Molecules and Solids* (McGraw-Hill Book Company, Inc., New York, 1965), Vol. II, p. 124.
[13] R. W. G. Wyckoff, *Crystal Structures* (Interscience Publishers, Inc., New York, 1963), Vol. I.
[14] We have used atomic units (a.u.) in which $e^2=2$, $m=\frac{1}{2}$ and $\hbar=1$. Energies are in rydbergs (13.595 eV) and distances in Bohr radii (0.5292 Å).
[15] J. Worster and N. H. March, Solid State Commun. **2**, 245 (1964).

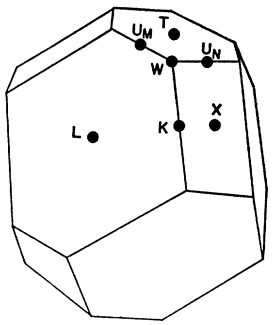


FIG. 1. Brillouin zone for the rhombohedral crystal structure of mercury.

to have almost exactly the same energy (differing by only 0.01 eV/atom). It is also interesting in this regard that the coordination number for liquid mercury as found by x-ray diffraction techniques[16] is 10.0 and the average atomic distance (at 28°C) is 5.76 a.u. One expects the electronic environments in the liquid and solid to be quite similar except, of course, for properties which result from Bragg reflections due to periodicity in the crystal.

The crystal potential was constructed by superposing atomic potentials and charge densities centered on the lattice sites. The relativistic self-consistent-field calculations of Liberman, *et al.*[17] for the configuration $5d^{10}6s^2$ were used. Exchange was treated throughout using the Slater free-electron approximation. Inside the APW sphere radius (2.718 a.u.) the potential was spherically symmetric, and outside it was flattened into the muffin-tin form. The reciprocal lattice vectors used in the basic set were selected so that all the energy levels throughout the zone had converged to an accuracy of better than 0.005 Ry. This required 19 reciprocal lattice vectors, yielding a secular determinant of order 38. The matrix elements in the RAPW method have been discussed previously.[18] This aspect of the calculation will not be repeated here.

## III. RESULTS AND DISCUSSION

### The Fermi Surface

The relativistic energy bands are shown in Figs. 2 and 3. They are free-electron-like with splittings due to the combined effect of the crystal potential and the spin-orbit interaction. The dashed region near the bottom of the band and the inset in Fig. 3 will be discussed in the next section. Because mercury is divalent, the Fermi energy will be near the top of the first band. We have used the dHvA data of Brandt and Rayne[5] to estimate the value shown in Figs. 2 and 3. Their data indicate that the Fermi energy must lie above the lower level at $X$ and below the maximum in this band between $X$

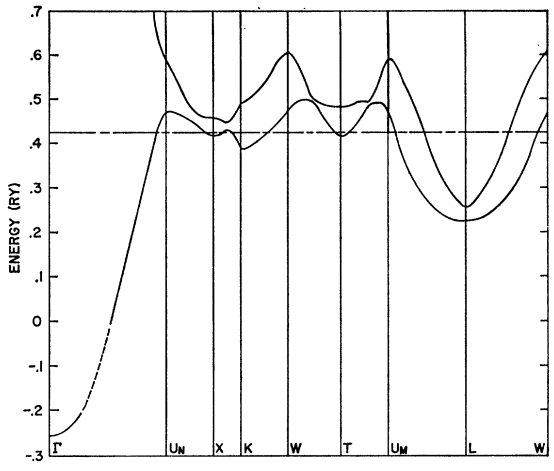


FIG. 2. Relativistic energy bands for mercury.

and $K$. This fixes the Fermi energy between 0.670 and 0.685 Ry (measured from the bottom of the band at −0.255 Ry). The value $E_F=0.680$ gives good agreement with the dHvA frequency associated with this portion of the Fermi surface. We have used this approximate value of the Fermi energy to determine the intersections of the Fermi surface with the Brillouin zone faces as shown in Fig. 4. This Fermi surface is topologically equivalent to the model proposed by Brandt and Rayne[5] to explain their dHvA data. In the first zone there is a multiply connected hole surface which includes most of the $T$ and $X$ faces except for regions near the points $T$ and $X$. A schematic representation of this part of the Fermi surface is shown in Fig. 5. In the second zone there are lens-shaped electron surfaces centered on the points $L$ and oriented with maximum cross section in the $L$-faces.

In discussing a noncubic crystal structure such as rhombohedral mercury, it is important to be very careful in the use of crystallographic notations to indicate planes and directions. Before proceeding to a

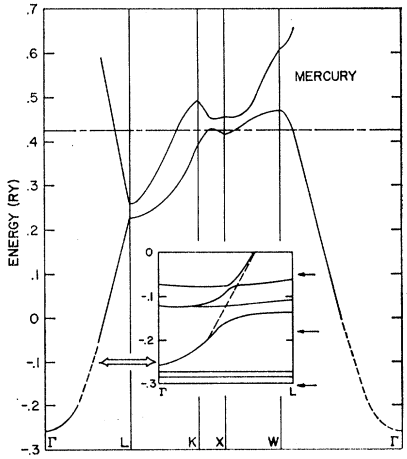


FIG. 3. Relativistic energy bands for mercury.

[16] C. N. J. Wagner, H. Ocken, and M. L. Joshi, United States Atomic Energy Commission Report No. TID-20304, 1964 (unpublished).
[17] D. Liberman, J. T. Waber, and Don T. Cromer, Phys. Rev. **137**, A27 (1965).
[18] T. L. Loucks, Phys. Rev. **143**, 506 (1966).

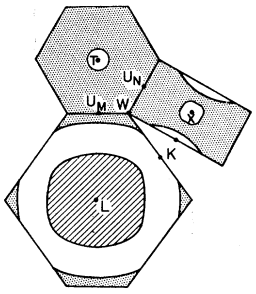


FIG. 4. Intersections of Fermi surface with Brillouin zone faces.

comparison between the Fermi surface and the various experimental results, let us review briefly the nomenclature. The Brillouin zone shown in Fig. 1 was constructed in the usual manner by finding the region contained by the perpendicular bisectors of reciprocal lattice vectors. The basic reciprocal lattice vectors in rhombohedral mercury have the following $(x,y,z)$ coordinates:

$$\begin{aligned}\mathbf{b}_1&=(1.111,\ 0,\ 0.4990)\\ \mathbf{b}_2&=(-0.5553,\ 0.9618,\ 0.4990)\\ \mathbf{b}_3&=(-0.5553,\ -0.9618,\ 0.4990).\end{aligned}\tag{1}$$

All reciprocal lattice vectors can be designated by

$$(l,m,n)=l\mathbf{b}_1+m\mathbf{b}_2+n\mathbf{b}_3.$$

Some of the reciprocal lattice vectors used in constructing the Brillouin zone are indicated in Fig. 6.

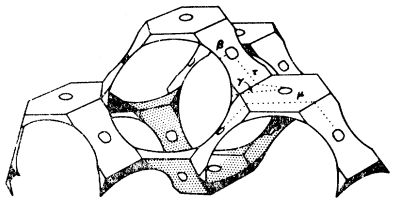

FIG. 5. Schematic representation of the multiply connected first zone hole surface of mercury showing closed orbits.

Of course, the reciprocal lattice point $(l,m,n)$ defines the set of lattice planes $(lmn)$ in the direct lattice.

Some of the experimental results we will discuss involve the orientation of a magnetic field with respect to the crystal. However, in discussing the Fermi surface we shall be concerned with the orientation of the magnetic field with respect to the Brillouin zone. Directions corresponding to lines of atoms in the crystal will be specified in the usual manner by $[lmn]$. To determine the orientation these directions have with respect to the Fermi surface, we find the normal to the plane in reciprocal space which contains all the reciprocal lattice vectors $(l'm'n')$ such that the inner product with $[lmn]$ vanishes. For instance, the direction $[00\bar{1}]$ has zero inner product with the reciprocal lattice vectors (110), (100) and $(1\bar{1}0)$. The normal to the plane in reciprocal space which contains these three vectors is parallel to the zone edge $WKW$. This is shown in Fig. 7. We notice that the three orthogonal directions [111], $[11\bar{2}]$, and $[1\bar{1}0]$ (called trigonal, bisectrix, and binary, respectively), specify the same directions relative to the Brillouin zone as the corresponding reciprocal lattice vectors (111), $(11\bar{2})$ and $(1\bar{1}0)$. However [110] and (110) have different orientations with respect to the Brillouin zone, as do also $[00\bar{1}]$ and $(00\bar{1})$. In the following discussion we shall frequently refer to the orientation of a magnetic field with respect to the Fermi surface. It is hoped that Fig. 7 will help the reader avoid some of the confusion which arises from the use of many different forms of brackets. We shall also use the accepted convention that $\langle lmn\rangle$ represents $[lmn]$ and all

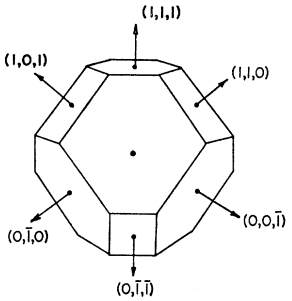


FIG. 6. Reciprocal lattice vectors corresponding to faces of the Brillouin zone. (1,0,0) normal to the plane of the figure.

equivalent directions; similarly, $\{lmn\}$ represents $(lmn)$ and all equivalent planes (or reciprocal lattice vectors). As a final remark, it should be noticed that although in Fig. 7 the binary direction $[1\bar{1}0]$ is perpendicular to the bisectrix direction $[11\bar{2}]$, the equivalent direction $[10\bar{1}]$ (one of the set $\langle 1\bar{1}0\rangle$) makes an angle of 30° with the $[11\bar{2}]$ direction.

The experimental evidence for the electron lenses can be seen in the dHvA data of Brandt and Rayne.[8] The curve marked $\alpha$ in Fig. 8a corresponds to a side view of one of the sets of lenses. With field oriented in the $[10\bar{1}]$ direction, the minimum cross section of the lenses is observed. From the theoretical Fermi surface we calculate the corresponding frequency to be 37.4 $\times 10^6$ G compared to the observed value of $32.2\times 10^6$ G. As the field is rotated to either the [100] or the $[00\bar{1}]$ direction, the frequency increases by about 10% because the Fermi surface pulls out toward the point $K$ as shown in Fig. 4. The observed frequencies also increase by about this same amount as can be seen in Fig. 8(a).

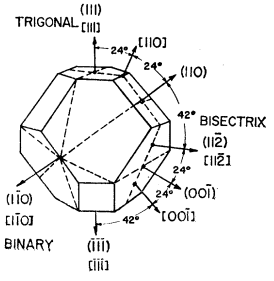


FIG. 7. The orientation of certain crystallographic directions with respect to the Brillouin zone.

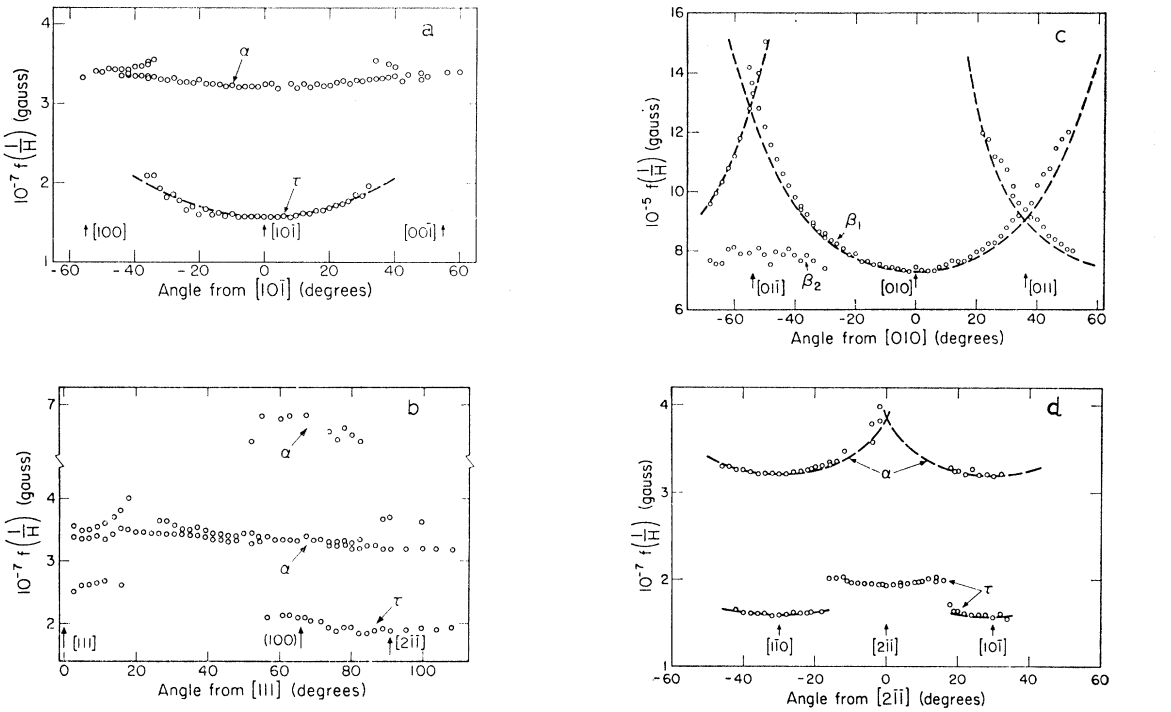


FIG. 8. de Haas–van Alphen data of Brandt and Rayne (Ref. 8) (a) magnetic field in the (010) plane. Dashed curve corresponds to the behavior expected from cylinders oriented along ⟨100⟩. (b) Magnetic field in the (01$\bar{1}$) plane. (c) Magnetic field in the (100) plane. Dashed curves correspond to the behavior expected from cylinders oriented along ⟨100⟩. (d) Magnetic field in the (111) plane. Dashed curves correspond to the behavior expected from ellipsoidal lenses on the {100} zone faces.

With the field in either the [100] or [00$\bar{1}$] direction there are two sets of lenses with the same orientation relative to the field. As the field is rotated toward the [10$\bar{1}$] direction, one of the sets assumes an orientation such that the maximum cross section of the lenses is approached. We calculate this maximum to correspond to the frequency $107\times10^6$ G. The frequency corresponding to this set of lenses should therefore rise very sharply over the angular range given in Fig. 8(a). We see only the first part of this expected signal in the experimental results near [100] and [00$\bar{1}$].

The maximum cross section of the lenses should be observed for field orientation in the {100} direction. In Fig. 8(b) we show the experimental results of Brandt and Rayne for the magnetic field in a plane perpendicular to the binary direction, i.e., lying in the mirror plane. The scale of the figure is too small to include the predicted value of $107\times10^6$ G. However, a scatter of signals near the (100) direction with frequency around $68\times10^6$ G have been observed. These were assigned to the lens orbit by Brandt and Rayne. We agree that this is a possible interpretation. It would require a little bending of the theoretical bands, but no more than has been necessary in other similar situations. It would simply require the lenses to be thicker and have a smaller maximum cross section than we have calculated. But it is tempting for us to believe the bands and look for an alternative interpretation of the data. It is, for instance, possible that the lenses do have a maximum cross section corresponding to a frequency of about $107\times10^6$ G, and that they simply have not been observed. There is no experimental data which goes continuously from the maximum cross section to the side view of the lenses. This interpretation would leave the frequencies around $68\times10^6$ G in Fig. 8(b) unexplained. It is always possible that these are mixing frequencies or even harmonics ($68\times10^6$ G is not too different from twice the side-view frequencies which range from 32 to $35\times10^6$ G at this orientation). And, as we shall point out later, there are also orbits on the hole surface which yield frequencies of this same order of magnitude. In our opinion this assignment of orbits is not yet completely resolved.

The multiply connected hole surface is shown in Figs. 4 and 5. All but one of the closed orbits on this surface have previously been classified by Brandt and Rayne. The surface covers most of the $T$ and $X$ faces except for small regions around the points $T$ and $X$. There is experimental evidence confirming the presence of these small openings. As noticed by Brandt and Rayne, in the vicinity of $X$ and $K$ the hole surface may be approximated by two parallel cylinders oriented in the ⟨001⟩ directions (parallel to $K$-$W$ in Fig. 1). The experimental frequencies corresponding to these cylindrical regions are designated $\beta_1$ in Fig. 8(c). With

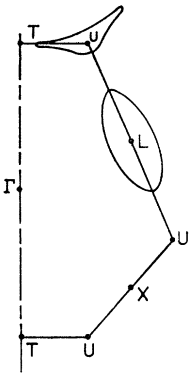


FIG. 9. View of theoretical Fermi surface corresponding to minimum cross sections of the electron lenses and the $\tau$ orbit on the hole surface. $[10\bar{1}]$ normal to the plane of the figure.

magnetic field in the [010] direction, the orbits around one set of cylinders have minimum cross section. (There are, of course, three sets of cylinders corresponding to the three equivalent ⟨001⟩ directions. The other two sets do not support closed orbits at this field orientation.) As the field is rotated toward $[01\bar{1}]$, this cross section increases and one of the other sets begins to support closed orbits; these two sets acquire the same orientation with respect to the magnetic field at $[01\bar{1}]$. This leads to crossing of the frequencies at $[01\bar{1}]$ as can be seen in Fig. 8(c). Notice that Brandt and Rayne have made this interpretation quite plausible by calculating the angular dependence to be expected from cylindrical surfaces oriented in the ⟨001⟩ direction. As mentioned earlier, it was this feature of the Fermi surface which we used to fix the Fermi energy. It was chosen such that the intersection with the energy bands between the points $X$ and $K$ gave the same size cylinder as was experimentally observed. As a last comment on the experimental results shown in Fig. 8(c), the frequencies indicated as $\beta_2$ do not correspond to any portion of the theoretical Fermi surface. Unless they correspond to difference frequencies, their presence is unexplainable.

The other openings in the hole surface occur around the $T$ points. The experimental evidence for this feature of the Fermi surface can be found in closed orbits which thread through these openings and the openings at $X$. Brandt and Rayne have designated these as $\tau$ orbits, and they can be seen in Figs. 8(a) and 8(b). Additional experimental results are shown in Fig. 8(d). In Fig. 9 we show the shape of this orbit corresponding to its minimum cross sectional area (magnetic field in ⟨$10\bar{1}$⟩ direction). The theoretical surface predicts a frequency of $13.8\times10^6$ G compared to the experimental results of $15.8\times10^6$ G obtained from Fig. 8(a). As the field is rotated in the (111) plane [see Fig. 8(d)] away from the $[1\bar{1}0]$ direction, the Fermi surface supports this closed orbit only over a small angular range. From Fig. 4 we predict closed orbits for a range of about 9–10° on either side of $[1\bar{1}0]$. This is in good agreement with the two lower sets of experimental frequencies shown in Fig. 8(d) and designated as $\tau$ orbits. The frequencies around $[2\bar{1}\bar{1}]$ are also designated as $\tau$ in Fig. 8(d), but actually correspond to a different orbit. This orbit threads through the opening at $T$ and around the point $W$ where the cylinders spread out as they join together (Fig. 5). We prefer to designate this orbit as $\gamma$ in order to distinguish it from the $\tau$ orbits. There is a break in the data between the $\gamma$ and $\tau$ orbits for the small angular range in which the orbits run along the cylinders and are either open orbits or extended orbits. These open orbits are discussed later. The experimental frequencies designated by $\tau$ in Fig. 8(b) also correspond to the $\gamma$ orbits. The observed angular dependence is consistent with the Fermi surface model. In this same figure there are frequencies in the range of $27\times10^6$ G for fields oriented near [111]. We cannot find extremal areas on the theoretical Fermi surface to explain these.

There is one additional closed orbit which has not previously been discussed. We designate this as a $\mu$ orbit. It goes across the $T$ faces and through two of the openings centered at the $X$ points as shown in Fig. 5. We estimate that for the field orientation in the $(01\bar{1})$ plane this orbit should exist for directions between $[2\bar{1}\bar{1}]$ and [100]. The frequency should increase between $[2\bar{1}\bar{1}]$ and [100] with a value of about $45\times10^6$ G in the (100) direction. There is no clear evidence that these orbits have been observed experimentally. However, in Fig. 8(d) we notice that around $[2\bar{1}\bar{1}]$ the data gets a little sparse where we would expect the $\mu$ orbit to have about the same frequency as the lens orbit. This could be the result of beating between these two signals. Also, in Fig. 8(b) there are frequencies around $[2\bar{1}\bar{1}]$ which could be due to this orbit. This aspect of the Fermi surface (as well as the exact size of the lenses) will have to be determined by further experimental work from which these orbits can be clearly identified.

Both Dixon and Datars[6] and Brandt and Rayne[8] have measured effective masses for orbits on the cylindrical portions of the hole surface. The two groups reported results for different magnetic field traverses. In both cases, however, the angular dependence of the results was consistent with the theoretical Fermi surface and with the de Haas–van Alphen results. It is somewhat disturbing, however, that with the field oriented in the (110) direction (a measurement both groups made) Dixon and Datars reported $m=0.79$ while Brandt and Rayne gave 0.23. The former was based on Azbel'-Kaner cyclotron resonance measurements, the latter on the temperature variation of the amplitude of the torque oscillations from de Haas-van Alphen measurements. *Note added in proof.* In a private communication from W. R. Datars we have been informed that their earlier effective mass measurements[6] actually corresponded to the electron lenses. This removes the apparent discrepancy between their results and those of Brandt and Rayne.[8]

The Fermi surface supports two sets of open orbits. An example of each is shown in Fig. 10. The set desig-

TABLE I. Distances to neighboring atoms in zinc (hcp) and mercury (rhombohedral).

| Number atoms | Distance (a.u.) Zinc | Mercury |
|---|---|---|
| 6 | 5.02 | 5.65 |
| 6 | 5.52 | 6.55 |
| 6 | 7.44 | 8.65 |

nated A was first predicted by Brandt and Rayne[5] and later observed by Dixon and Datars[6] in their transverse magnetoresistance results. These are shown in Fig. 11. Using the lattice constants for mercury we calculate that for the configuration in Fig. 11 the magnetoresistance should saturate with the field 38° from (110) toward (100). The path of the resulting open orbit is shown in Fig. 12. The direction of motion in reciprocal space is parallel to the (010) direction. The other set of open orbits, designated *B* in Fig. 10, were observed by Dishman and Rayne.[7] In their paper can be found a complete discussion of both sets of open orbits. *Note added in proof.* Dixon and Datars (to be published) have found evidence of other sets of open orbits which can be related to the model shown in Fig. 10.

In the above discussion we have shown that the theoretical Fermi surface based on the RAPW calculation is consistent with the available experimental evidence. However, the theoretical calculation was performed after the experimental evidence had already been interpreted on the basis of a modification of the free-electron model. Brandt and Rayne[8] used a parameterized pseudopotential fit of their de Haas-van Alphen data to determine a Fermi surface model. It is interesting that these authors did not find it necessary to include the spin-orbit interaction as Anderson and Gold[19] had done for lead. Because the symmetry is lower in the rhombohedral lattice, the crystal field splits levels which would be degenerate in the fcc lattice if the spin-orbit interaction were not included. Therefore, the pseudopotential parameters for mercury contain the combined effect of the weak crystal potential and the spin-orbit interaction. It is gratifying that the relativistic calculation using an *ad hoc* potential reproduces the essential features of the Fermi surface model based on experimental results.

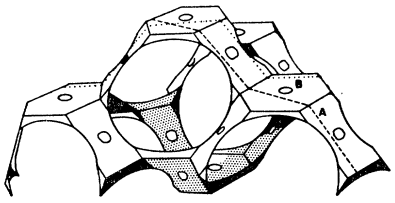

FIG. 10. Schematic representation of the multiply connected first-zone hole surface of mercury showing an example of each of the two sets of open orbits.

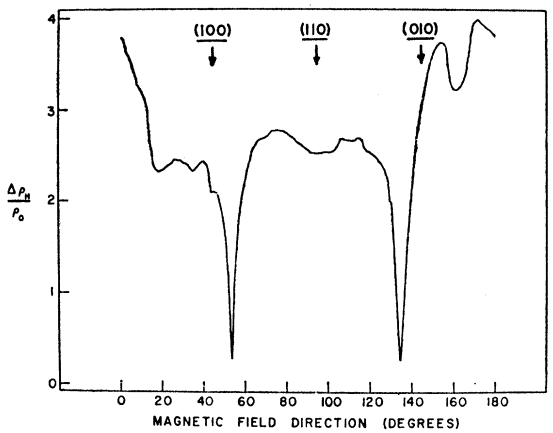


FIG. 11. Transverse magnetoresistance results of Dixon and Datars (Ref. 6) with the magnetic field lying in a plane normal to [001].

### The *d* Bands

A result which at first surprised us was the location of the filled 5*d* bands. The inset in Fig. 3 shows three of these bands cutting across the bottom of the 6*s*-6*p* bands and the other two just below it. Mattheiss[20] has calculated the energy bands for zinc (hcp) and found that the 3*d* band was about 0.5 Ry below the bottom of the 4*s*-4*p* bands. This is in contrast to the neighboring element copper (fcc) in which the 3*d* band occupies energies ranging from about $\frac{1}{2}$ to $\frac{4}{5}$ of the Fermi energy.

There are several factors which could effect the relative position of the *d* bands. One is the overlap from neighboring atoms in the crystal. In performing atomic self-consistent field calculations for transition elements we have observed the effect that changes in the outer portion of the potential have on the relative positions of *s* and *d* levels. Modifications which make the potential more binding in the outer portion of the atomic potential lower the energy of the outer *d* level with respect to

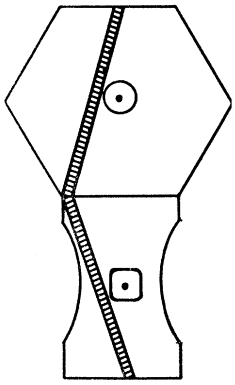

FIG. 12. Path of the open orbit on the first-zone hole surface which gives rise to the saturation in the magnetoresistance as shown in Fig. 11.

[19] J. R. Anderson and A. V. Gold, Phys. Rev. **139**, A1459 (1965).

[20] L. F. Mattheiss, Phys. Rev. **134**, A970 (1964).

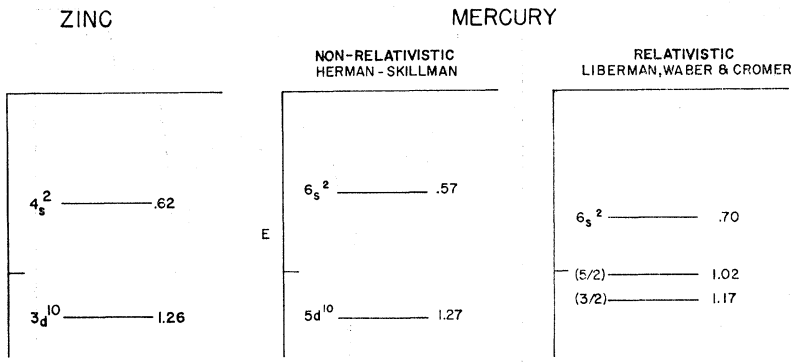


FIG. 13. Results of atomic self-consistent-field calculations for mercury and zinc.

the $s$ level. The superpositioning procedure used to form the muffin-tin potential tends to make it more binding in the outer region. We thus expect that if the overlap from neighboring atoms is different for mercury and zinc, it would affect the relative positions of the $d$ bands. Unfortunately, it is not an easy matter to separate out the various contributions to this effect. For instance, the atomic radius of mercury is, roughly, 25% greater than that of zinc. On the other hand, the two elements have different crystal structures and different nearest-neighbor distances. Distances to the 18 nearest neighbors for the two lattices are given in Table I. We see that the 12 nearest neighbors are, roughly, 25% closer in zinc than in mercury. Certainly this is a very crude argument, but we might conclude that although the mercury atoms are larger, they are correspondingly further away from their nearest neighbors, and consequently the overlap would be about the same for the two elements. We therefore do not believe this to be an important factor in determining the position of the $d$ bands.

There is an entirely different effect, however, which can account for the shift in the $d$-band position. In Fig. 13, we have shown the results of atomic self-consistent-field calculations for mercury and zinc. The nonrelativistic calculations for these two elements by Herman and Skillman[21] give almost identical results for the outer $s$ and $d$ levels. However, the relativistic calculation by Liberman *et al.*[17] for mercury show the $5d$ levels considerably higher in energy with respect to the $6s$ level. Liberman *et al.* have explained the shift in the $d$ level as an indirect relativistic effect. The states of lower angular momentum are more tightly bound by the effective potential in the relativistic calculation.[17] We used the relativistic atomic potential to construct the crystal potential and believe this accounts for the position of the $d$ bands.

Since the location of the $d$ bands seems plausible, we look for experimental evidence to support the result. We do not know of any such experiments on solid mercury. However, the reflection spectrum of liquid mercury has been measured recently by Wilson and Rice,[22] and their results tend to confirm the location of the $d$ bands. They were able to account for the imaginary part of the dielectric constant in the energy range below 7 eV by extending the Drude theory to include the effects of electron-ion interactions. This energy range corresponds to the free-electron-like portion of our energy bands above the $d$ bands. There are three absorption peaks in the imaginary part of the dielectric constant which occur in the energy range corresponding to our $d$ bands. The experimental results are shown in Fig. 14(a). The positions of the peaks relative to the Fermi energy are shown by arrows along

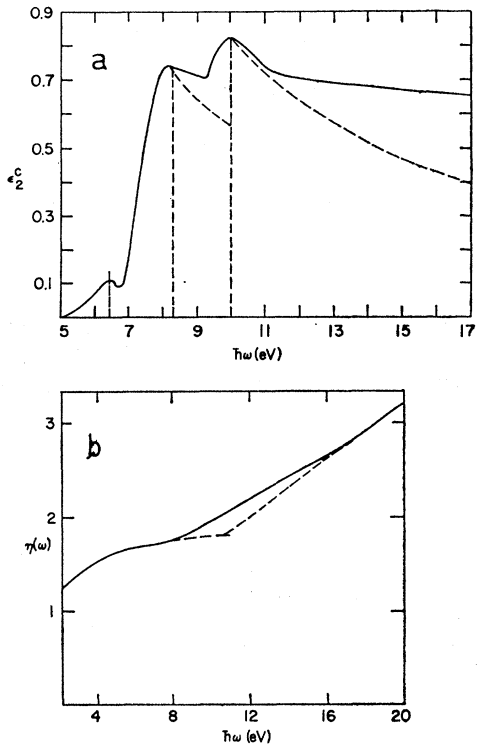


FIG. 14. (a) Results of Wilson and Rice (Ref. 22) deduced from their reflectance data for liquid mercury. Excess absorption over that predicted by the Drude theory as a function of photon energy. (b) Test of the Kramers-Kronig sum rule.

[21] F. Herman and S. Skillman, *Atomic Structure Calculations* (Prentice-Hall, Inc., Englewood Cliffs, New Jersey, 1963).
[22] E. G. Wilson and Stuart A. Rice, Phys. Rev. 145, 55 (1966).

the inset portion of Fig. 3. It is apparent that the absorptions are due to transitions between these $d$ bands and the states above the Fermi energy. In Fig. 14(b) we see evidence that some of the $d$ bands cut across the bottom of the $s$-$p$ band. The ordinate of this figure can be regarded as the number of electrons which contribute to the dielectric constant up to the energy $\hbar\omega$. We see that it tends toward the value 2, but at the energy corresponding to the position of the $d$ bands there is an abrupt change in slope. Thus, the $d$-band absorptions begin contributing before the states at the bottom of the conduction band.

Wilson and Rice[22] have interpreted their results in terms of $5d$ core electrons which are split by the spin-orbit interaction. They point out that the energy difference between the $J=\frac{3}{2}$ and $J=\frac{5}{2}$ states of Hg(II) in the configuration $5d^9 6s^2$ is 1.87 eV compared to the splitting of 1.7 eV between the absorption peaks in Fig. 14(a). We would like to point out that the crystal field can equally well account for the splitting. We have noted that the $d$ bands shown in the inset in Fig. 3 extend over the same energy range as the observed absorption peaks. The $d$ bands are split by the combined effects of the spin-orbit interaction and the crystal field (lack of spherical symmetry due to the neighboring atoms). To emphasize this we have also calculated these bands in the nonrelativistic limit. The results are shown in Fig. 15. The $d$ bands are still split into two sets; however, the effect is now entirely due to the crystal field. In the crystal, therefore, the splitting of the $d$ bands is a combined effect of both the spin-orbit interaction and the crystal field. The same should be true in the liquid state, since, as we have pointed out earlier, the average electronic environment due to nearest neighbors should be quite similar in the two states.

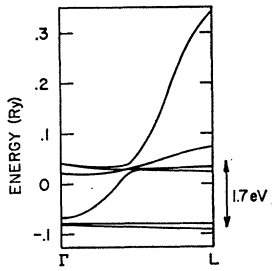


FIG. 15. Nonrelativistic energy bands for mercury near the bottom of the conduction band.

## ACKNOWLEDGMENTS

We are grateful to J. A. Rayne for originally stimulating our interest in this subject and for graciously providing us with unpublished results done in collaboration with G. B. Brandt. We have also benefitted from discussions with A. E. Dixon and W. R. Datars. Although there has been no specific reference made in the text, we have benefitted greatly from the recent research done by N. F. Mott on the liquid state of mercury and other metals. A special note of thanks is due A. R. Mackintosh with whom we have enjoyed daily discussions on most of the aspects of our research projects. His assistance is greatly appreciated.